

Stability of Repulsive Bose-Einstein Condensates in a Periodic Potential

J. C. Bronski¹, L. D. Carr², B. Deconinck³, J. N. Kutz^{3*}, and K. Promislow⁴

¹*Department of Mathematics, University of Illinois Urbana-Champaign, Urbana, IL 61801, USA*

²*Department of Physics, University of Washington, Seattle, WA 98195-1560, USA*

³*Department of Applied Mathematics, University of Washington, Seattle, WA 98195-2420, USA*

⁴*Department of Mathematics, Simon Fraser University, Burnaby, B.C., CANADA V5A 1S6*

The cubic nonlinear Schrödinger equation with repulsive nonlinearity and an elliptic function potential models a quasi-one-dimensional repulsive dilute gas Bose–Einstein condensate trapped in a standing light wave. New families of stationary solutions are presented. Some of these solutions have neither an analog in the linear Schrödinger equation nor in the integrable nonlinear Schrödinger equation. Their stability is examined using analytic and numerical methods. All trivial-phase stable solutions are deformations of the ground state of the linear Schrödinger equation. Our results show that a large number of condensed atoms is sufficient to form a stable, periodic condensate. Physically, this implies stability of states near the Thomas–Fermi limit.

I. INTRODUCTION

Recent experiments on dilute–gas Bose–Einstein condensates (BECs) have generated great interest in macroscopic quantum phenomena [1,2] in both the theoretical and experimental physics community. Such BECs are experimentally realized when certain gases are super-cooled below a critical temperature and trapped in electromagnetic fields [3]. Many BEC experiments use harmonic confinement. Recently, however, there has been much interest in sinusoidal confinement of repulsive BECs using standing light waves. Such BECs have been used to study phase coherence [4–6] and matter-wave diffraction [7]. They have also been predicted to apply to quantum logic [8,9], matter-wave transport [10], and matter-wave gratings. In this paper, we consider the dynamics and stability of repulsive BECs trapped in standing light waves.

A mean–field description for the macroscopic BEC wavefunction is constructed using the Hartree–Fock approximation [11] and results in the Gross–Pitaevskii equation [12,13]. The dimensions of the BEC play an important role: 1D, 2D, and 3D BECs all behave in a radically different manner [14,15]. In the quasi-1D regime, the Gross–Pitaevskii equation reduces to the 1D nonlinear Schrödinger equation (NLS) with an external potential. This regime holds when the transverse dimensions of the condensate are on the order of its healing length and the longitudinal dimension is much longer than its transverse dimensions [16,17]. In this regime the BEC remains phase coherent and the governing equations are one-dimensional. This is in contrast to a truly 1D mean-field theory which requires transverse dimensions on the order of or less than the atomic interaction length.

The recent trapping of a BEC in a hollow blue-detuned laser beam [23] demonstrates that a quasi-1D BEC is experimentally realizable. A variety of other experi-

ments [1,18,19,23–26] are also modeled by the 1D NLS with an external potential. Upon rescaling, the governing evolution is given by

$$i\psi_t = -\frac{1}{2}\psi_{xx} + |\psi|^2\psi + V(x)\psi, \quad (1)$$

where $\psi(x, t)$ is the macroscopic wave function of the condensate and $V(x)$ is an experimentally generated macroscopic potential. Confinement in a standing light wave results in $V(x)$ being periodic. In a recent experiment [4,5], a shallow harmonic potential was applied in addition to a standing light wave. The standing light wave in this case was sufficiently intense so that the condensate was strongly localized in each well. This is referred to as the tight-binding regime. Additionally, the apparatus was tilted vertically so that gravity caused tunneling between wells. Our theoretical findings consider the complementary experiment in which the condensate is free to move between wells. With the advent of quasi-1D, cylindrical geometries [23], additional harmonic confinement is no longer necessary and the BEC dynamics considered here are applicable.

To model the quasi-1D confinement produced by a standing light wave, we use the periodic potential

$$V(x) = -V_0 \operatorname{sn}^2(x, k) \quad (2)$$

where $\operatorname{sn}(x, k)$ denotes the Jacobian elliptic sine function [27] with elliptic modulus $0 \leq k \leq 1$. In the limit $k = 0$ the potential is sinusoidal and thus $V(x)$ is a standing light wave. For intermediate values (e.g. $k < 0.9$) the potential closely resembles the sinusoidal behavior and thus provides a good approximation to a standing light wave. Finally, for $k \rightarrow 1^-$, $V(x)$ becomes an array of well-separated hyperbolic secant potential barriers or wells. The potential is plotted in Fig. 1 for values of $k = 0, 0.9, 0.999$ and 0.999999 . Only for k very near one (e.g. $k > 0.999$) does the solution appear visibly elliptic.

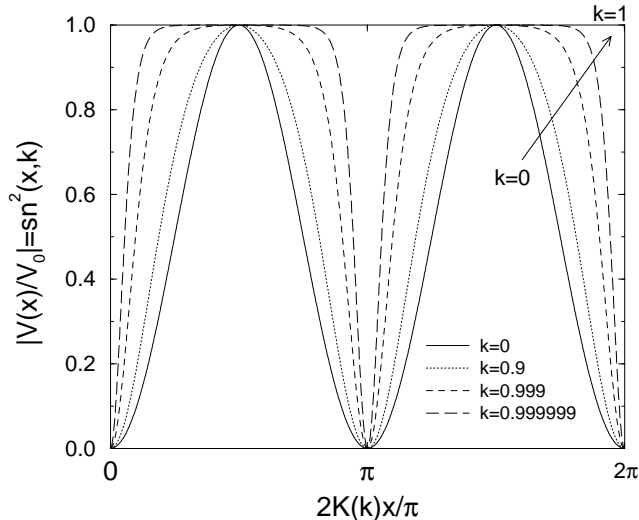


FIG. 1. The $\text{sn}^2(x, k)$ structure of the potential for varying values of k . Note that the x -coordinate has been scaled by the period of the elliptic function. This period approaches infinity as $k \rightarrow 1$. Since $\text{sn}(x, k)$ is periodic in x with period $4K(k) = 4 \int_0^{\pi/2} d\alpha / \sqrt{1 - k^2 \sin^2 \alpha}$, $V(x)$ is periodic in x with period $2K(k)$.

The freedom in choosing k allows us to consider much more general potentials than considered previously [28–31] and allows for great flexibility in considering a wide variety of physically realizable potentials.

The paper is outlined as follows: in the next section we derive and consider various properties and limits of two types of explicit solutions of Eq. (1) with (2). Section III develops the analytic framework for the linear stability properties of the new solutions of Sec. II. The stability results are confirmed by numerical computations. In certain cases, the stability analysis is intractable and we rely solely on simulations to determine stability. We conclude the paper in Sec. IV with a brief summary and highlights of the primary results of the paper and their consequences for BEC dynamics and confinement.

II. STATIONARY SOLUTIONS

Equation (1) with $V(x) = 0$ is an integrable equation and many explicit solutions corresponding to various boundary conditions are known. A comprehensive overview of these solutions is found in [32]. If $V(x) \neq 0$, the NLS is not integrable. In this case, only small classes of explicit solutions can most likely be obtained. Our choice of potential (2) is motivated by the form of the stationary solution of the NLS with $V(x) = 0$. An overview of these stationary solutions and their properties is found in [16]. At present, we restrict our attention to stationary solutions of Eq. (1), *i.e.*, solutions whose time-dependence is restricted to

$$\psi(x, t) = r(x) \exp(-i\omega t + i\theta(x)). \quad (3)$$

If $\theta_x \equiv 0$, then the solution is referred to as having trivial phase and we choose $\theta(x) = 0$. Substituting the ansatz Eq. (3) in Eq. (1) and dividing out the exponential factor results in two equations: one from the real part and one from the imaginary part. The second equation can be integrated:

$$\theta(x) = c \int_0^x \frac{dx'}{r^2(x')}, \quad (4)$$

where c is a constant of integration. Note that $\theta(x)$ is a monotonous function of x . Substitution of this result in the remaining equation gives

$$\omega r^4(x) = \frac{c^2}{2} - \frac{r^3(x)r''(x)}{2} + r^6(x) - V_0 \text{sn}^2(x, k)r^4(x). \quad (5)$$

The following subsections describe two classes of solutions of this equation.

Type A

1. Derivation

For these solutions, $r^2(x)$ is a quadratic function of $\text{sn}(x, k)$:

$$r^2(x) = A \text{sn}^2(x, k) + B. \quad (6)$$

Substituting this ansatz in Eq. (5) and equating the coefficients of equal powers of $\text{sn}(x, k)$ results in relations among the solution parameters ω, c, A and B and the equation parameters V_0 and k . These are

$$\omega = \frac{1}{2} \left(1 + k^2 + 3B - \frac{BV_0}{V_0 + k^2} \right), \quad (7a)$$

$$c^2 = B \left(1 + \frac{B}{V_0 + k^2} \right) (V_0 + k^2 + Bk^2), \quad (7b)$$

$$A = V_0 + k^2. \quad (7c)$$

For a given potential $V(x)$, this solution class has one free parameter B which plays the role of a constant background level or offset. The freedom in choosing the potential gives a total of three free parameters: V_0, k and B .

The requirements that both $r^2(x)$ and c^2 are positive imposes conditions on the domain of these parameters:

$$V_0 \geq -k^2, \quad B \geq 0, \quad \text{or} \quad (8a)$$

$$V_0 \leq -k^2, \quad -(V_0 + k^2) \leq B \leq -\left(1 + \frac{V_0}{k^2}\right). \quad (8b)$$

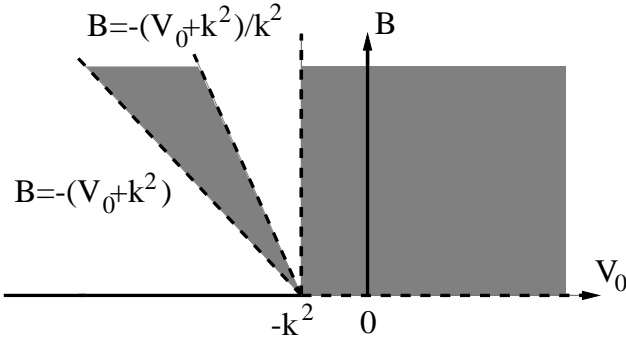


FIG. 2. The region of validity of the solutions of Type A is displayed shaded for a fixed value of k . The edges of these regions correspond to various trivial phase solutions.

The region of validity of these solutions is displayed in Fig. 2.

For typical values of V_0 , k and B , the above equations give rise to solutions of Eq. (1) which are not periodic in x : $r(x)$ is periodic with period $2K(k)$, whereas $\exp(i\theta(x))$ is periodic with period $T = \theta^{-1}(2\pi)$. In general these two periods $2K(k)$ and T are not commensurable. Thus, requiring periodic solutions results in another condition, namely $2K(k)/T = p/q$, for two positive integers p and q . The most convenient way to express this phase quantization condition is to assume the potential (*i.e.*, V_0 and k) is given, and to consider values of B for which the quantization condition is satisfied. Introducing $\beta = B/(V_0 + k^2)$, we find

$$\pm \frac{\sqrt{\beta(1+\beta)(1+k^2\beta)}}{\pi} \int_0^{K(k)} \frac{dx}{\text{sn}(x,k)^2 + \beta} = \frac{p}{q}. \quad (9)$$

This equation is solved for β , after which $B = \beta(V_0 + k^2)$. For numerical simulations, the number of periods of the potential is set. This determines q , limiting the number of solutions of Eq. (9). Solutions with the same periodicity as the potential require $p/q = 1$.

Note that solutions of Type A reduce to stationary solutions of Eqs. (1) and (2) with $V_0 = 0$. Furthermore, all stationary solutions of the integrable equation are obtained as limits of solutions of Type A.

2. Limits and Properties

The properties of these solutions are best understood by considering their various limit cases.

The trivial phase case: The solutions of Type A have trivial phase when $c = 0$. Since c^2 has three factors which are linear in B (see Eq. (7)), there are three choices of B for which this occurs: $B = 0$, $B = -(V_0 + k^2)$ and $B = -(V_0 + k^2)/k^2$. These possibilities are three of the four boundary lines of the region of validity in Fig. 2. Note that the remaining boundary line ($V_0 = -k^2$) corresponds to $r^2(x) = B$, which gives rise to a plane wave

solution. Using Jacobian elliptic function identities [27], one finds that the three other boundary lines give rise to simplified solution forms: $B = 0$ gives

$$r(x) = \sqrt{V_0 + k^2} \text{sn}(x, k), \quad \omega = \frac{1 + k^2}{2}. \quad (10)$$

$B = -(V_0 + k^2)$ gives

$$r(x) = \sqrt{-(V_0 + k^2)} \text{cn}(x, k), \quad \omega = \frac{1}{2} - V_0 - k^2, \quad (11)$$

where $\text{cn}(x, k)$ denotes the Jacobian elliptic cosine function. Lastly, $B = -(V_0 + k^2)/k^2$ gives

$$r(x) = \frac{\sqrt{-(V_0 + k^2)}}{k} \text{dn}(x, k), \quad \omega = -1 - \frac{V_0}{k^2} + \frac{k^2}{2}, \quad (12)$$

where $\text{dn}(x, k)$ denotes the third Jacobian elliptic function. Solution (10) is valid for $V_0 \geq -k^2$, whereas the other two solutions (11) and (12) are valid for $V_0 \leq -k^2$. The amplitude of these solutions as a function of potential strength V_0 is shown in Fig. 3.

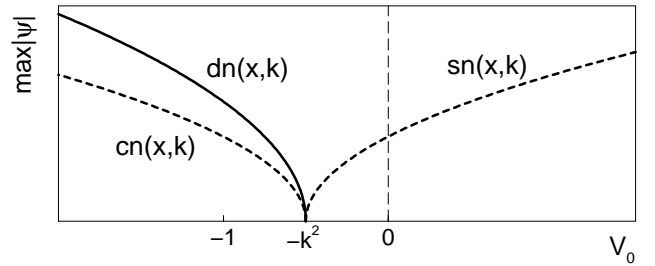


FIG. 3. The amplitude of the trivial phase solutions of Type A versus the potential strength V_0 .

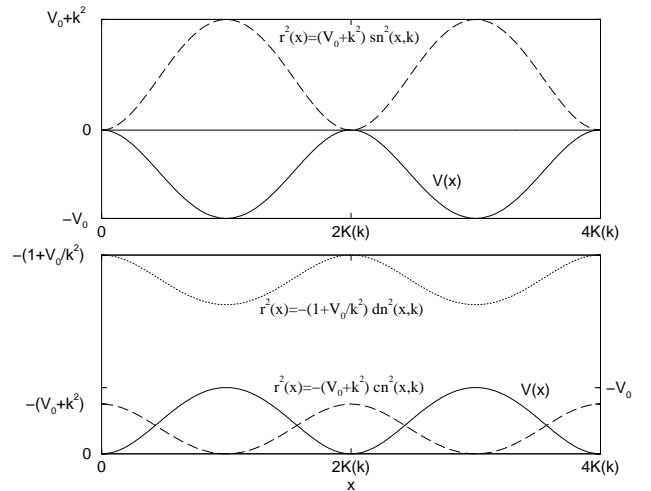


FIG. 4. Trivial phase solutions for $k = 0.5$. $V(x)$ is indicated with a solid line. For the top figure $V_0 = 1$. For the bottom figure $V_0 = -1$.

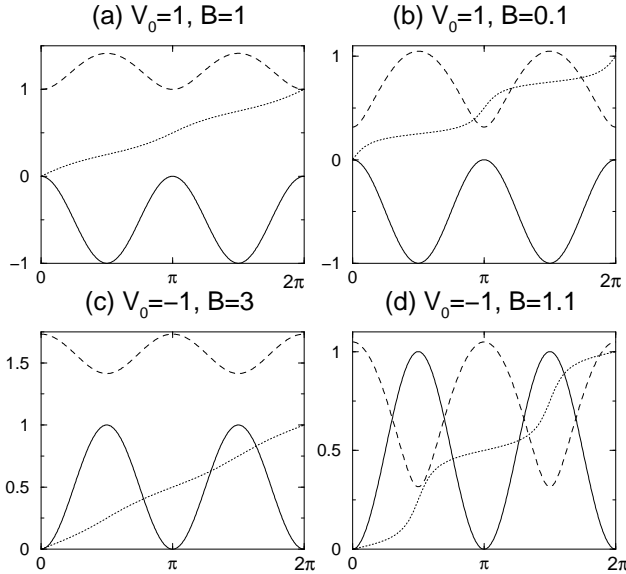


FIG. 5. Phase and amplitude of the trigonometric solutions. For all these figures, the solid line denotes $V(x)$, the dashed line is $r(x)$ and the dotted line is $\theta(x)/(2\pi)$. Note that $\theta(x)$ becomes piecewise constant, as B approaches the boundary of the region of validity. Far away from this boundary, $\theta(x)$ is essentially linear.

Both $\text{cn}(x, k)$ and $\text{sn}(x, k)$ have zero average as functions of x and lie in $[-1, 1]$. On the other hand, $\text{dn}(x, k)$ has nonzero average. Its range is $[\sqrt{1-k^2}, 1]$. Furthermore, $\text{cn}(x, k)$ and $\text{sn}(x, k)$ are periodic in x with period $4K(k)$, whereas $\text{dn}(x, k)$ is periodic with period $2K(k)$. These properties matter greatly for the stability analysis, as will be seen in Section 3. Some solutions with trivial phase are shown in Fig. 4.

The trigonometric limit: In the limit $k \rightarrow 0$, the elliptic functions reduce to trigonometric functions and $V(x) = -V_0 \sin^2(x) = (V_0/2) \cos(2x) - V_0/2$. Then

$$r^2(x) = V_0 \sin^2(x) + B, \quad \omega = \frac{1}{2} + B. \quad (13)$$

In this case, the phase integral Eq. (4) results in

$$\tan(\theta(x)) = \pm \sqrt{1 + V_0/B} \tan(x). \quad (14)$$

Note that this formula guarantees that the resulting solution is periodic with the same period as the potential, so no phase quantization is required. In the trigonometric limit, the wedge between the two regions of validity in Fig. 2 disappears. This is no surprise, as in this limit, $\text{dn}(x, k) \rightarrow 1$, and the third trivial phase solution reduces to a plane wave solution. The cornerpoint of the region of validity also moves to the origin. Some trigonometric solutions are illustrated in Fig. 5.

The solitary wave limit: $k = 1$. In this limit the elliptic functions reduce to hyperbolic functions. Specifically, $\text{sn}(x, k) = \tanh(x)$. Hence in this limit, the potential has only a single well or a single peak. Then $V_0 < 0$

gives rise to a repulsive potential, whereas $V_0 > 0$ gives rise to an attractive potential: $V(x) = -V_0 \tanh^2(x)$. In this case the phase $\theta(x)$ of Eq. (4) can be calculated explicitly:

$$r^2(x) = (V_0 + 1) \tanh^2(x) + B, \quad (15a)$$

$$\theta(x) = \sqrt{\frac{B}{V_0 + 1}} x + \arctan\left(\sqrt{\frac{V_0 + 1}{B}} \tanh(x)\right), \quad (15b)$$

which is valid for $V_0 > -1$ and $B > 0$. This solution is a stationary solitary wave of depression on a positive background. It is a deformation of the gray soliton solution of the NLS equation with repulsive nonlinearity. Note that these solutions can exist with an attractive potential provided $-1 < V_0 < 0$. Two solutions with repulsive potential are illustrated in Fig. 6a-b. Another solution is valid for $B = -(V_0 + 1) > 0$: $r(x) = \sqrt{-(V_0 + 1)} \text{sech}(x)$ and $\theta(x) = 0$. This solution represents a stationary elevated solitary wave. It is reminiscent of the bright soliton solution of the NLS equation with attractive nonlinearity. This solution is shown in Fig. 6c. A surprising consequence of considering Eq. (1) is that the potential strength V_0 acts as a switch between the equation with repulsive and attractive nonlinearity, as illustrated by these solitary wave solutions.

Understanding the solitary wave limit facilitates the understanding of what occurs for $k \rightarrow 1$. In this case the solutions of Type A reduce to a periodic train of solitons with exponentially small interactions as illustrated in Fig. 6d.

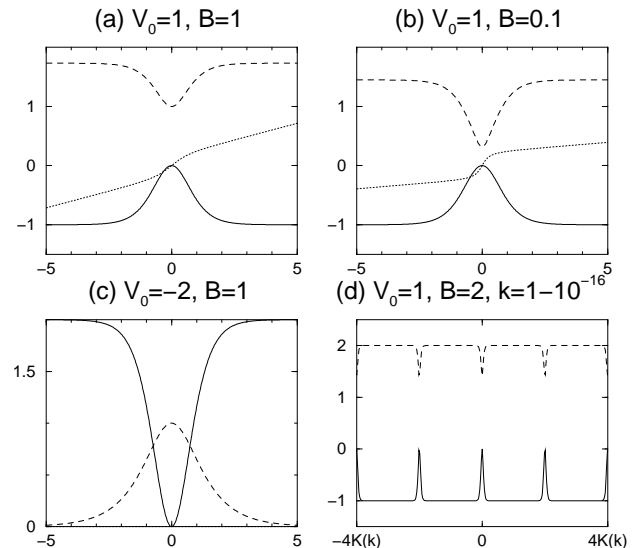


FIG. 6. Solutions with $k=1$ (a,b,c) or $k \rightarrow 1$ (d). The solid line denotes $V(x)$, the dashed line is $r(x)$ and the dotted line is $\theta(x)/2\pi$. In (d), a value of $k = 1 - 10^{-16}$ was used.

Type B

1. Derivation

For these solutions, $r^2(x)$ is linear in $\text{cn}(x, k)$ or $\text{dn}(x, k)$. First we discuss the solution with $\text{cn}(x, k)$. The quantities associated with this solution will be denoted with a subindex 1. The quantities associated with the $\text{dn}(x, k)$ solution receive a subindex 2.

Substituting

$$r_1^2(x) = a_1 \text{cn}(x, k) + b_1, \quad (16)$$

in Eq. (5) and equating different powers of $\text{cn}(x, k)$ gives the relations:

$$V_0 = -\frac{3}{8}k^2, \quad (17a)$$

$$\omega_1 = \frac{1}{8}(1 + k^2) + \frac{6a_1^2}{k^2}, \quad (17b)$$

$$c_1^2 = \frac{a_1^2}{4k^6}(16a_1^2 - k^4)(16a_1^2 + k^2 - k^4), \quad (17c)$$

$$b_1 = \frac{4a_1^2}{k^2}. \quad (17d)$$

The class of potentials Eq. (2) is restricted by the first of these relations so that V_0 is in the narrow range $-3k^2/8 \leq V_0 \leq 0$. The solution class now depends on one free amplitude parameter a_1 and the free equation parameter k .

The region of validity of this solution is, as before, determined by the requirements $c_1^2 \geq 0$ and $r_1^2(x) \geq 0$:

$$|a_1| \geq \frac{k^2}{4}. \quad (18)$$

The period of $r_1(x)$ is twice the period of the potential. Requiring periodicity in x of this first solution of Type B gives

$$\pm \frac{\sqrt{(\beta_1^2 - k^2)(\beta_1^2 + 1 - k^2)}}{4\pi} \int_0^{2K(k)} \frac{dx}{4\beta_1 + k \text{cn}(x, k)} = \frac{p}{q}. \quad (19)$$

For given k and integers p, q , this equation is solved for β_1 , from which $a_1 = \beta_1 k/4$.

The $\text{dn}(x, k)$ solutions are found by substituting

$$r_2^2(x) = a_2 \text{dn}(x, k) + b_2, \quad (20)$$

in Eq. (5). Equating different powers of $\text{dn}(x, k)$ imposes the following constraints on the parameters:

$$V_0 = -\frac{3}{8}k^2, \quad (21a)$$

$$\omega_2 = \frac{1}{8}(1 + k^2) + 6a_2^2, \quad (21b)$$

$$c_2^2 = \frac{a_2^2}{4}(16a_2^2 - 1)(16a_2^2 + k^2 - 1), \quad (21c)$$

$$b_2 = 4a_2^2. \quad (21d)$$

The class of potentials (2) is restricted as for the previous solution by the first of these relations. The solution class again depends on one free amplitude parameter a_2 and the free equation parameter k .

The region of validity of this solution is once more determined by the requirements $c_2^2 \geq 0$ and $r_2^2(x) \geq 0$:

$$|a_2| \geq \frac{1}{4} \quad \text{or} \quad 0 \leq a_2 \leq \frac{\sqrt{1 - k^2}}{4}. \quad (22)$$

The period of $r_2(x)$ is equal to the period of the potential. Requiring periodicity in x of this second solution of Type B gives

$$\pm \frac{\sqrt{(16a_2^2 - 1)(16a_2^2 + k^2 - 1)}}{\pi} \int_0^{K(k)} \frac{dx}{4a_2 + \text{dn}(x, k)} = \frac{p}{q}. \quad (23)$$

For given k and integers p, q , this equation needs to be solved to determine a_2 .

In contrast to solutions of Type A, solutions of Type B do not have a nontrivial trigonometric limit. In fact, for solutions of Type B, this limit is identical to the limit in which the potential strength $V_0 = -3k^2/8$ approaches zero. Thus it is clear that the solutions of Type B have no analogue in the integrable nonlinear Schrödinger equation. However, other interesting limits do exist.

2. Limits and Properties

The trivial phase case: Trivial phase corresponds to $c = 0$. This occurs precisely at the boundaries of the regions of validity. For the first solution of Type B, there are two possibilities: $a_1 = k^2/4$ or $a_1 = -k^2/4$. By replacing x by $x + 2K(k)$, one sees that these two possibilities are completely equivalent, so only the first one needs to be considered:

$$r_1^2(x) = \frac{k^2}{4}(1 + \text{cn}(x, k)), \quad \omega_1 = \frac{1}{8} + \frac{k^2}{2}. \quad (24)$$

For the second solution, there are four possibilities: $a_2 = 1/4$, $a_2 = -1/4$, $a_2 = 0$ and $a_2 = \sqrt{1 - k^2}/4$. The third one of these results in a zero solution. The others give interesting trivial phase solutions. For $a_2 = 1/4$,

$$r_2^2(x) = \frac{1}{4}(1 + \text{dn}(x, k)), \quad \omega_2 = \frac{1}{2} + \frac{k^2}{8}. \quad (25)$$

The case $a_2 = -1/4$ gives

$$r_2^2(x) = \frac{1}{4}(1 - \text{dn}(x, k)), \quad \omega_2 = \frac{1}{2} + \frac{k^2}{8}. \quad (26)$$

Finally, for $a_2 = \sqrt{1-k^2}/4$,

$$r_2^2(x) = \frac{\sqrt{1-k^2}}{4} (\text{dn}(x, k) + \sqrt{1-k^2}), \quad \omega_2 = \frac{1-k^2}{2}. \quad (27)$$

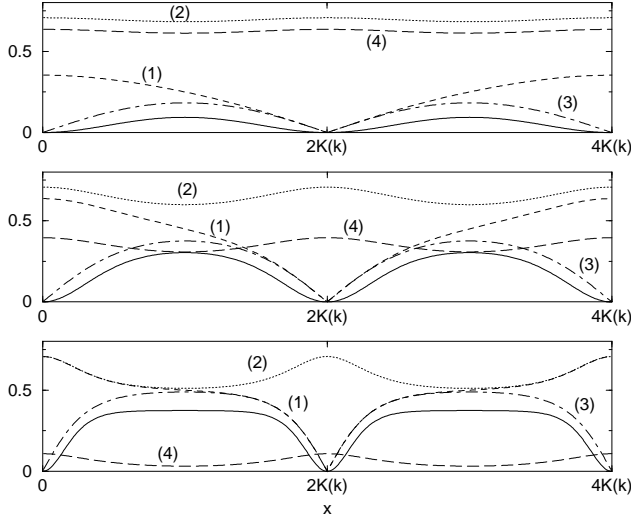


FIG. 7. Solutions of Type B with trivial phase. The figures correspond to, from top to bottom, $k = 0.5$, $k = 0.9$ and $k = 0.999$. The potential is indicated with a solid line. The other curves are: (1) $|r_1(x)|$ with $a_2 = k^2/4$, (2) $r_2(x)$ with $a_2 = 1/4$, (3) $|r_2(x)|$ with $a_2 = -1/4$ and (4) $r_2(x)$ with $a_2 = \sqrt{1-k^2}/4$.

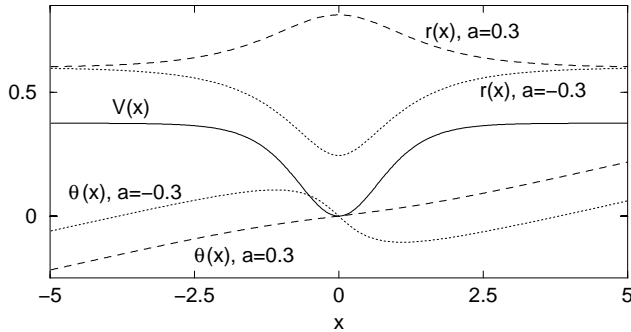


FIG. 8. Solitary wave solutions of Type B. The potential is indicated with a solid line. The dashed line solution corresponds to $a = 0.3$, the dotted line to $a = -0.3$.

These solutions are shown in Fig. 7.

The solitary wave limit: In this limit $V_0 = -3/8$ and the potential is $V(x) = 3 \tanh(x)^2/8$. Since both $\text{cn}(x, k) = \text{sech}(x)$ and $\text{dn}(x, k) = \text{sech}(x)$ when $k = 1$, $r_1(x) = r_2(x)$ in the solitary wave limit. Their ranges of validity also share the same limit: $|a| \geq 1/4$ with $a = a_1 = a_2$. The phase can be calculated explicitly and the solitary wave solution of Type B is

$$r^2(x) = 4a^2 + a \text{sech}(x), \quad (28a)$$

$$\theta(x) = \pm \frac{x\sqrt{16a^2-1}}{2} \mp \arctan\left(\sqrt{\frac{4a-1}{4a+1}} \tanh\frac{x}{2}\right). \quad (28b)$$

The region of validity consists of two separated regions: $a \geq 1/4$ and $a \leq -1/4$. In the first region, the solution is a stationary elevated solitary wave with a constant background $4a^2$. In the second region $a \leq -1/4$ and the solution is a stationary solitary wave of depression with a constant background $4a^2$. These solitary wave solutions are illustrated in Fig. 8

As for the solutions of type A, the solitary wave limit gives an idea of the behavior of the solution for values of $k \rightarrow 1$, where the solution behaves as a periodic array of solitons with exponentially small interactions.

III. STABILITY

We have found a large number of new solutions to the governing Eqs. (1) and (2). However, only solutions that are stable can be observed in experiments. In this section, we consider the stability of the different solutions. Both analytical and numerical results are presented for the solutions with trivial phase. In contrast, only numerical results are presented for the nontrivial phase cases.

We first consider the linear stability of the solution (3). To do so, consider perturbations of the exact solutions of the form

$$\psi(x, t) = (r(x) + \epsilon\phi(x, t)) \exp[i(\theta(x) - \omega t)] \quad (29)$$

where $\epsilon \ll 1$ is a small parameter. Collecting terms at $O(\epsilon)$ gives the linearized equation. In terms of the real and imaginary parts $\mathbf{U} = (U_1, U_2)^t = (\text{Re}[\phi], \text{Im}[\phi])^t$ the linearized evolution is given by:

$$\mathbf{U}_t = J L \mathbf{U} = J \begin{pmatrix} L_+ & -S \\ S & L_- \end{pmatrix} \mathbf{U}, \quad (30)$$

where

$$L_+ = -\frac{1}{2} \left(\partial_x^2 - \frac{c^2}{r^4(x)} \right) + 3r^2(x) + V(x) - \omega, \quad (31a)$$

$$L_- = -\frac{1}{2} \left(\partial_x^2 - \frac{c^2}{r^4(x)} \right) + r^2(x) + V(x) - \omega, \quad (31b)$$

$$S = \frac{c}{r(x)} \partial_x \frac{1}{r(x)}, \quad (31c)$$

and $J = \begin{pmatrix} 0 & -1 \\ 1 & 0 \end{pmatrix}$ is a skew-symmetric matrix. The operators L , L_+ and L_- are Hermitian while S is anti-Hermitian. Considering solutions of the form $\mathbf{U}(x, t) = \hat{\mathbf{U}}(x) \exp(\lambda t)$ gives the eigenvalue problem

$$\mathcal{L} \hat{\mathbf{U}} = \lambda \hat{\mathbf{U}}, \quad (32)$$

where $\mathcal{L} = JL$ and λ is complex. If all λ are imaginary, then linear stability is established. In contrast, if there is at least one eigenvalue with a positive real part, then instability results. Using the phase invariance $\psi \mapsto e^{i\gamma}\psi$ of Eq. (1), Noether's theorem [33] gives

$$\mathcal{L} \begin{pmatrix} 0 \\ r(x) \end{pmatrix} = 0, \quad (33)$$

which implies that $L_-r(x) = 0$. Thus $\lambda = 0$ is in the spectrum of L_- . For general solutions of the form (3), determining the spectrum of the associated linearized eigenvalue problem (30) is beyond the scope of current methods. However, some cases of trivial phase solutions ($c = 0$) are amenable to analysis.

The Hermitian operators L_{\pm} are periodic Schrödinger operators and thus the spectra of these operators is real and consists of bands of continuous spectrum contained in $[\lambda_{\pm}, \infty)$ [33]. Here λ_{\pm} denote the ground state eigenvalues of L_{\pm} respectively. They are given by

$$\lambda_{\pm} = \inf_{\|\phi\|=1} \langle \phi | L_{\pm} | \phi \rangle, \quad (34)$$

where $\|\phi\|^2 = \langle \phi | \phi \rangle$. From the relation $L_+ = L_- + 2r^2(x)$ it follows that $\lambda_+ > \lambda_-$. Also $\lambda_- \leq 0$ since $\lambda = 0$ is an eigenvalue of L_- .

If $\lambda_+ > 0$, then L_+ is positive, so we can define the positive square root, $L_+^{\frac{1}{2}}$, via the spectral theorem [33], and hence the Hermitian operator $H = L_+^{\frac{1}{2}}L_-L_+^{\frac{1}{2}}$ can be constructed. The eigenvalue problem for \mathcal{L} in Eq. (32) is then equivalent to

$$(H + \lambda^2)\varphi = 0, \quad (35)$$

with $\varphi = L_+^{\frac{1}{2}}\hat{U}_1$. Denote the left-most point of the spectrum of H by μ_0 . If $\mu_0 \geq 0$ then $\lambda^2 < 0$ and the eigenvalues of \mathcal{L} are imaginary and linear stability results. Since $H = L_+^{\frac{1}{2}}L_-L_+^{\frac{1}{2}}$ and $L_+^{\frac{1}{2}}$ is positive, $\mu_0 \geq 0$ if and only if L_- is non-negative. In contrast, if $\mu_0 < 0$ then $\lambda^2 > 0$ and \mathcal{L} has at least one pair of real eigenvalues with opposite sign. This shows the existence of a growing mode leading to instability of the solution.

Three distinct cases are possible for linear stability

- If $r(x) > 0$ then $r(x)$ is the ground state of L_- [33], and Eq. (33) implies $\lambda_- = 0$ and hence $\lambda_+ > 0$. Thus the solution (3) is linearly stable.
- If $r(x)$ has a zero, it is no longer the ground state [33] and $\lambda_- < 0$. Thus there exists a ψ_0 such that $\langle \psi_0 | L_- | \psi_0 \rangle < 0$. If in addition $\lambda_+ > 0$, then we can construct $\phi = L_+^{-\frac{1}{2}}\psi_0 / \|L_+^{-\frac{1}{2}}\psi_0\|$ which gives $\langle \phi | H | \phi \rangle < 0$. Hence $\mu_0 < 0$ and \mathcal{L} has positive, real eigenvalues so that the solution (3) is linearly unstable.

- For λ_- and λ_+ both negative the situation is indefinite and our methods are insufficient to determine linear stability or instability.

In what follows, these results are applied to the Type A and B trivial phase solutions constructed in the preceding section. Specifically, we construct the operators L_-

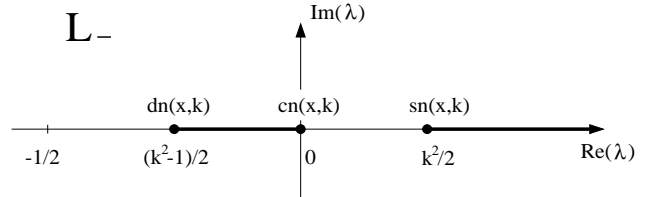


FIG. 9. The spectrum of L_- for the Type A $\text{cn}(x, k)$ trivial phase solution.

and L_+ for each solution, which allows us to use one of the above criteria. The analytical results are accompanied by direct computations on the nonlinear governing Eqs. (1) and (2). For all computational simulations, twelve spatial periods are used. However, to better illustrate the dynamics, typically four spatial periods are plotted. Moreover, all computations are performed with white noise included in the initial data.

A. Trivial Phase: Type A

1. $\text{cn}(x, k)$

For the $\text{cn}(x, k)$ solution the L_{\pm} operators are

$$L_+ = -\frac{1}{2}\partial_x^2 - (2V_0 + 3k^2)\text{cn}^2(x, k) + k^2 - \frac{1}{2} \quad (36a)$$

$$L_- = -\frac{1}{2}\partial_x^2 - k^2\text{cn}^2(x, k) + k^2 - \frac{1}{2}, \quad (36b)$$

with $V_0 < -k^2$. Note that L_- , which is independent of V_0 , is the classical 1-gap Lamé operator [32]. The spectrum of L_- can be calculated explicitly. The ground state eigenvalue is $\lambda_- = (k^2 - 1)/2$ with associated eigenfunction $\text{dn}(x, k)$. The elliptic functions $\text{cn}(x, k)$ and $\text{sn}(x, k)$ are also eigenfunctions of L_- . They are the first and second excited state and have eigenvalue 0 and $k^2/2$ respectively. These are the only eigenvalues and the spectrum consists of the bands $[(k^2 - 1)/2, 0] \cup [k^2/2, \infty)$. The spectrum is illustrated in Fig. 9.

Since $\text{dn}(x, k) > 0$ and $\lambda_- = (k^2 - 1)/2 < 0$ the arguments of the previous section imply that the $\text{cn}(x, k)$ wave is unstable whenever the operator $L_+ > 0$. It is clear from Eq. (36a) that L_+ is positive if $V_0 < -(k^2 + 1/4)$ and $k^2 > 1/2$. Thus, the $\text{cn}(x, k)$ wave is unstable for parameter values in this region. Moreover, this region can be enlarged to $V_0 < -(k^2 + 1)/2$ and $k^2 > 1/2$ by

observing that the ground state eigenvalue of an operator $L_0 + \gamma L_1$ is a convex function of γ : $\lambda = \Lambda(\gamma)$. This follows from the fact that the ground state eigenvalue is the minimizer of the Rayleigh quotient. Let $\alpha \in [0, 1]$, then

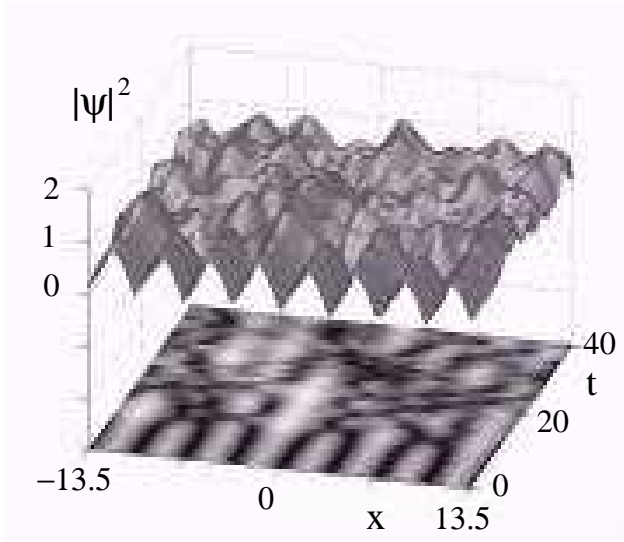


FIG. 10. Unstable evolution of a Type A $\text{cn}(x, k)$ solution given by Eq. (11) over 40 time units with $k = 0.5$ and $V_0 = -1.0$.

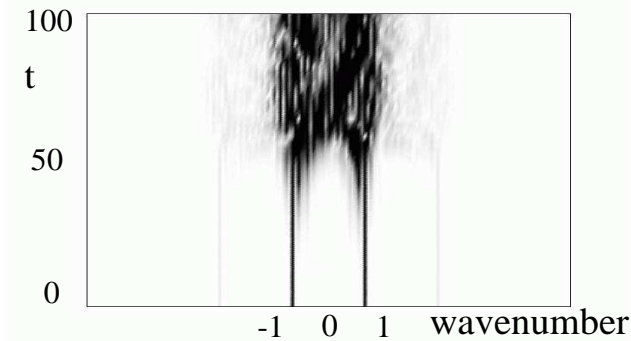


FIG. 11. Wavenumber spectrum evolution of a Type A $\text{cn}(x, k)$ solution given by Eq. (11) over 100 time units with $k = 0.5$ and $V_0 = -0.55$. The modal evolution shows the band of unstable modes which result from starting with the unstable $\text{cn}(x, k)$ solution. This shows that the instability occurs in a neighborhood of the dominant wavenumber of the stationary solution.

$$\begin{aligned}
& \Lambda(\alpha\gamma_1 + (1-\alpha)\gamma_2) \\
&= \inf_{\|\phi\|=1} \langle \phi | \alpha(L_0 + \gamma_1 L_1) + (1-\alpha)(L_0 + \gamma_2 L_1) | \phi \rangle \\
&\geq \alpha \inf_{\|\phi\|=1} \langle \phi | L_0 + \gamma_1 L_1 | \phi \rangle + (1-\alpha) \inf_{\|\phi\|=1} \langle \phi | L_0 + \gamma_2 L_1 | \phi \rangle \\
&= \alpha\Lambda(\gamma_1) + (1-\alpha)\Lambda(\gamma_2). \tag{37}
\end{aligned}$$

Now consider the ground state eigenvalue $\lambda_+ = \Lambda_+(V_0)$ and note that $\Lambda_+(-k^2) = (k^2 - 1)/2$ and $\Lambda_+(-3k^2/2) = k^2 - 1/2$. The line through these two points is given by $\Lambda_+(V_0) = -V_0 - (1 + k^2)/2$, so by convexity $\Lambda_+(V_0) \geq -V_0 - (1 + k^2)/2$ for $V_0 \in [-3k^2/2, -k^2]$. Thus, $\lambda_+ = \Lambda(V_0) \geq 0$ if $V_0 \leq -(1 + k^2)/2$.

If $k^2 < 1/2$, less is known. However the results of Weinstein and Keller [34] show that the ground state eigenvalue grows as $\lambda_+ \approx (2(1 - k^2)|V_0|)^{1/2} + k^2 - 1/2$ for $-V_0 \gg 1$. Hence for $k^2 \leq 1/2$ instability occurs for sufficiently negative V_0 .

The most unstable modes of the $\text{cn}(x, k)$ solution can be determined perturbatively when $\varepsilon = -2(V_0 + k^2) \ll 1$. This corresponds to a solution with small amplitude. Since $L_+ = L_- + \varepsilon \text{cn}^2(x, k)$, it follows that L_+ is not necessarily positive, disallowing the construction of H in Eq. (35). However, from Eq. (32), $L_+ L_- \hat{U}_2 = -\lambda^2 \hat{U}_2$, which offers an alternative to Eq. (35) to calculate the spectrum of Eq. (32). Let $\lambda = i\nu + \varepsilon\lambda_1$ and $\hat{U}_2 = \phi_\nu + \varepsilon\phi_1$, where ν is an eigenvalue of L_- and ϕ_ν is its associated normalized eigenfunction. Then a first order calculation using time-independent perturbation theory gives

$$\lambda^2 = -\nu^2 - \varepsilon\nu \langle \phi_\nu | \text{cn}^2(x, k) | \phi_\nu \rangle. \tag{38}$$

Thus, $\lambda^2 > 0$ only if $-\varepsilon \langle \phi_\nu | \text{cn}^2(x, k) | \phi_\nu \rangle < \nu < 0$. Hence, only modes ϕ_ν with ν in this band near zero are unstable. For these unstable modes, the eigenfunction ϕ_ν is approximately the zero mode $\text{cn}(x, k)$. Thus the onset of instability in the Fourier domain occurs near the wavenumbers of the $\text{cn}(x, k)$ solution. This is characteristic of a modulational instability

To illustrate this instability, we display in Fig. 10 the evolution of a $\text{cn}(x, k)$ solution over the time interval $t \in [0, 40]$ for $V_0 = -1.0$ and $k = 0.5$. The solution goes quickly unstable with the instability generated near the first wavenumber. This agrees with the analytical prediction. It is illustrated in the evolution of the wavenumber spectrum in Fig. 11. Here a close-up of the spectrum near wavenumber one is shown. This shows that the instability indeed occurs in a neighborhood of the dominant wavenumber of the stationary solution.

2. $\text{sn}(x, k)$

For the $\text{sn}(x, k)$ solutions the L_\pm operators are given by

$$L_+ = -\frac{1}{2}\partial_{xx} + (3k^2 + 2V_0)\text{sn}^2(x, k) - \frac{1+k^2}{2}, \tag{39a}$$

$$L_- = -\frac{1}{2}\partial_{xx} + k^2\text{sn}^2(x, k) - \frac{1+k^2}{2}. \tag{39b}$$

Again L_- is a 1-gap Lamé operator, differing from L_- for the $\text{cn}(x, k)$ solution only by a constant. The spectrum is given by $[-k^2/2, -1/2] \cup [0, \infty)$. It again follows from

the work of Weinstein and Keller [34] that for sufficiently large values of V_0 the ground state eigenvalue of L_- is approximately given by

$$\lambda_+ \approx (2V_0)^{\frac{1}{2}} - \frac{1+k^2}{2} \quad (40)$$

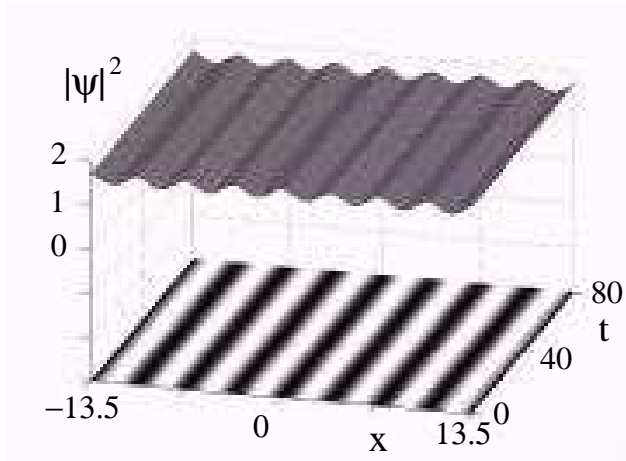


FIG. 12. Stable evolution of the Type A $\text{dn}(x, k)$ solutions given by Eq. (12) over 80 time units with $k = 0.5$ and $V_0 = -1.0$.

and thus L_+ is positive definite for sufficiently large V_0 . This, in turn, implies instability of the $\text{sn}(x, k)$ solution for sufficiently large V_0 , which corresponds to large amplitude solutions. The $\text{sn}(x, k)$ solution goes quickly unstable in a similar fashion to the $\text{cn}(x, k)$ solution (see Fig. 10).

3. $\text{dn}(x, k)$

From the previously established results, linear stability for the $\text{dn}(x, k)$ solutions follows immediately since $r(x) > 0$, because $\text{dn}(x, k)$ has no zeros. Thus in contrast to the $\text{cn}(x, k)$ and $\text{sn}(x, k)$ solutions, the $\text{dn}(x, k)$ solutions given by Eq. (12) are linearly stable. Figure 12 displays the evolution of a $\text{dn}(x, k)$ solution over the time interval $t \in [0, 80]$ for $V_0 = -1.0$ and $k = 0.5$. Although noise was added to the initial data, the solution shape persists and the solution is stable, as predicted analytically. For this case, the wavenumber spectrum is supported primarily by three modes: the zero mode which determines the offset, and two other modes which determine the oscillation frequency of the $\text{dn}(x, k)$ solution. Even with large perturbations, this solution persists. This indicates that the offset of a solution is important for its stability. This observation is reconfirmed for other stable solutions below.

B. Trivial Phase: Type B

1. $\text{cn}(x, k)$

The Type B trivial phase solution is obtained for $a_1 = \pm k^2/4$ and corresponding amplitude $|r(x)| = (k/2)\sqrt{1 + \text{cn}(x, k)}$. The solution $r(x)$ is not strictly positive. The operator L_+ is

$$L_+ = -\frac{1}{2}\partial_x^2 + \frac{k^2}{4} - \frac{1}{8} + \frac{3}{8}k^2 \text{sn}^2(x, k) + 3a_1 \text{cn}(x, k). \quad (41)$$

Thus we find that the situation is indeterminate.

Numerical simulations for the Type B $\text{cn}(x, k)$ solutions given by Eq. (24) are illustrated in Fig. 13. This figure displays the evolution of the $\text{cn}(x, k)$ branch of solution for $k = 0.5$ (top panel) and $k = 0.999$ (bottom panel) over the time interval $t \in [0, 800]$ and $t \in [0, 400]$ respectively for $V_0 = -3k^2/8$. For both $k = 0.5$ and $k = 0.999$ the solutions are unstable, but this instability manifests itself only after several hundred time units. Figure 14 shows the evolution of the wavenumber spectrum for both these cases. For $k = 0.5$, the onset of instability occurs near wavenumber one as is the case of Type A solutions. After 800 time units, the wavenumbers have only just begun to spread, causing the solution to

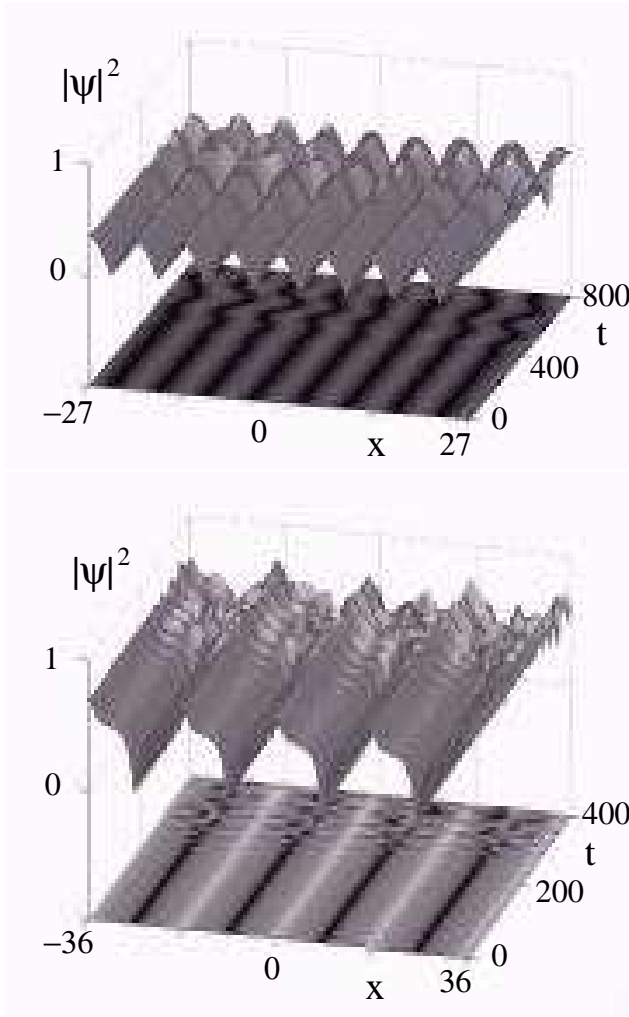


FIG. 13. Unstable evolution of the Type B $cn(x, k)$ solutions given by Eq. (24) for $k = 0.5$ (top panel) and $k = 0.999$ (bottom panel) for $a_1 = k^2/4$ and $V_0 = -3k^3/8$.

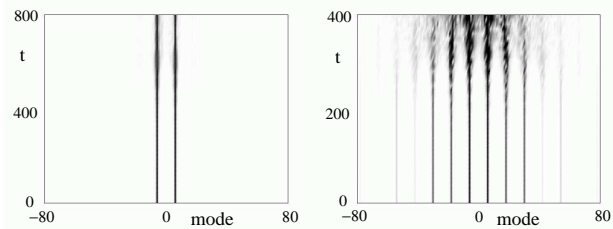


FIG. 14. Wavenumber spectrum evolution of a Type B $cn(x, k)$ solution given by Eq. (11) for $a_1 = k^2/4$ and corresponding to $k = 0.5$ (left panel) and $k = 0.999$ (right panel) of Fig 13. The evolution shows that the unstable band of modes is generated near wavenumber one and for $k = 0.999$ near wavenumber one and its harmonics.

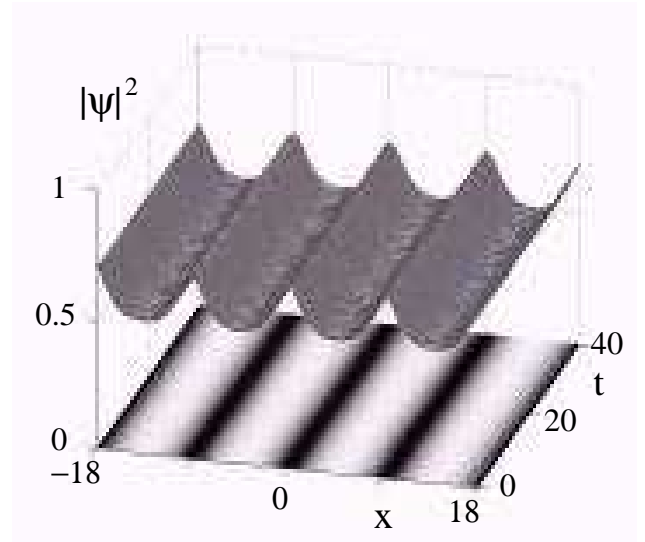


FIG. 15. Stable evolution of a Type B $dn(x, k)$ solution given by Eq. (25) for $k = 0.999$ and $a_2 = 1/4$.

destabilize. For $k = 0.999$, the solution is composed of a much larger number of wavenumbers which destabilize much more quickly than the $k = 0.5$ case. Here the instability is generated near wavenumber one and its harmonics.

2. $dn(x, k)$

The trivial phase $dn(x, k)$ solution requires $c = 0$ which is achieved for $a_2 = \pm 1/4$, $a_2 = 0$, or $a_2 = \sqrt{1 - k^2}/4$. Thus three distinct parameter regimes need to be considered. The relevant operators in this case are

$$L_+ = -\frac{1}{2}\partial_x^2 - \frac{k^2 + 1}{8} + 6a_2^2 + \frac{3k^2}{8}\text{sn}^2(x, k) + 3a_2\text{dn}(x, k), \quad (42a)$$

$$L_- = -\frac{1}{2}\partial_x^2 - \frac{k^2 + 1}{8} - 2a_2^2 + \frac{3k^2}{8}\text{sn}^2(x, k) + a_2\text{dn}(x, k). \quad (42b)$$

The case $a_2 = 1/4$ gives $L_-r(x) = 0$ with $r(x) > 0$. Hence from the linear stability criteria, these waves are stable for all values of k . As with the $a_2 = 1/4$ case, the regime where $a_2 = \sqrt{1 - k^2}/4$ gives a solution $r(x)$ which is strictly positive and is the ground state of L_- . Thus stability follows for all values of k . The last parameter regime, for which $a_2 = -1/4$, is indeterminate since both λ_- and λ_+ are negative and our linear stability analysis is inconclusive.

These analytic predictions are confirmed in Figs. 15–16. In Fig. 15 the evolution of a $dn(x, k)$ solution is shown for $a_2 = 1/4$ and $k = 0.999$. As predicted analytically, this parameter regime is stable for all k values. This simulation once again illustrates the importance of an offset for stabilizing the condensate [20]. In contrast to this

stable evolution, the case $a_2 = -1/4$ is unstable as illustrated in Fig. 16. The linear stability results in this case are indeterminate. However, the numerical simulations

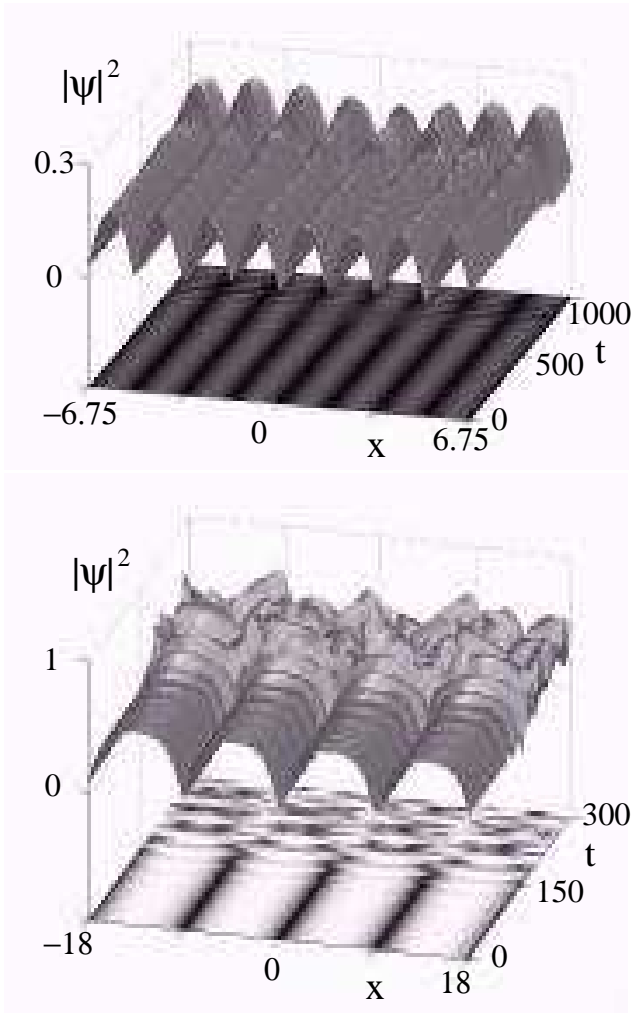


FIG. 16. Unstable evolution of a Type B $\text{dn}(x, k)$ solution given by Eq. (26) for $k = 0.5$ (top panel) and $k = 0.999$ (bottom panel) given $a_2 = -1/4$. In this case, there is no offset to stabilize the condensate.

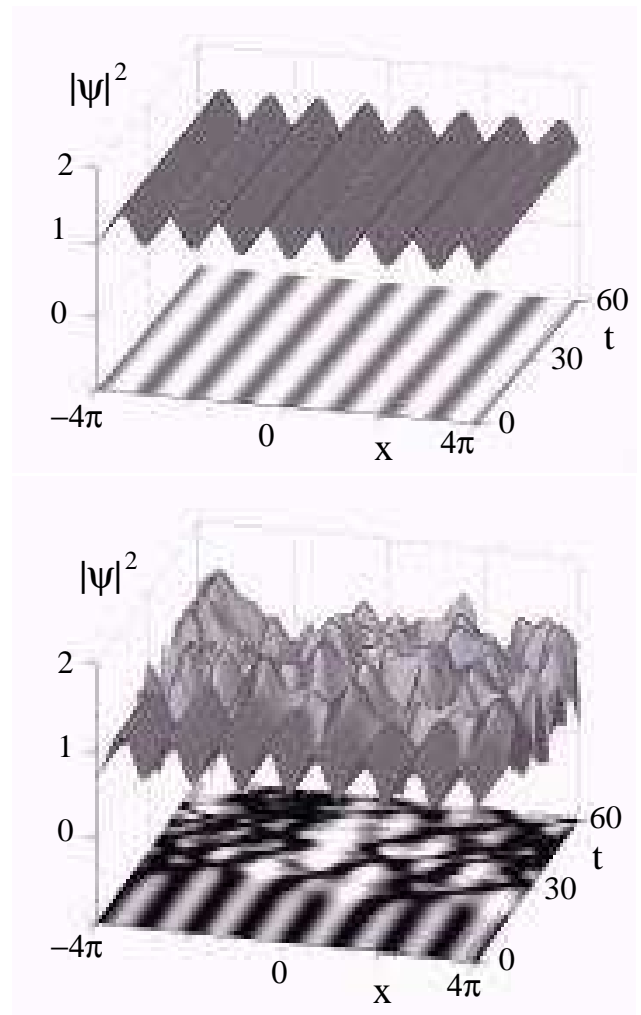


FIG. 17. Evolution of a nontrivial phase Type A solution with $V_0 = 1.0$ and $B = 1$ (top panel) and $B = 1/2$ (bottom panel). For B sufficiently large, the offset provided is able to stabilize the condensate whereas for B below a critical threshold the condensate destabilizes as shown for $B = 1/2$.

conclusively show the evolution to be unstable for all k values. For this case, the offset of the solution is insufficient to stabilize the condensate. We note that for small values of k , the onset of instability occurs after a very long time. Higher values of k result in instabilities on a much faster time scale. Finally, we consider the parameter regime for which $a_2 = \sqrt{1 - k^2}/4$. In this case, the analytic predictions once again suggest stability for all k values. We do not illustrate this case since it is qualitatively very similar to Fig. 16. However, in contrast to the $a_2 = 1/4$ case, for values of k close to one, there is a negligible amount of offset, distinguishing this stable case from previous ones. For these values of k , the solution has a small amplitude compared to the potential so that the behavior is essentially linear and stability is achieved because the condensate is trapped in the wells of the potential, as in ordinary quantum mechanics.

C. Nontrivial Phase

As stated at the beginning of Section III, determining the linear stability for nontrivial phase solutions is not amenable to analysis. This leads us to consider the stability of nontrivial phase solutions using numerical computations.

To begin, consider the trigonometric limit of the nontrivial phase solutions of Type A. These solutions are given by Eqs. (13) and (4). Figure 17 depicts the evolution of a pair of initial conditions with $V_0 = 1.0$ and for which $B = 1$ (top panel) and $B = 1/2$ (bottom panel). Since B determines the offset of the condensate, these numerical results show directly the importance of this offset for stability. In contrast, if the offset is too small, it is unable to stabilize the condensate.

For Type B solutions, qualitatively nothing changes from the dynamics illustrated for the trivial phase case. In particular, numerical simulations can be performed using exact solutions which are constructed subject to the phase quantization condition given by either Eq. (19) or (23). A numerical shooting method is used to find appropriate values of a_2 for which a phase-quantized, periodic solution exists. Once this is achieved, numerical simulations can easily be performed. Note that any integer value p is allowed as input for the phase quantization conditions, provided solutions exist for the parameter values. It turns out this imposes a lower bound on value of p . In the simulations, the actual value of p does not affect the stability of the solution. Increasing the phase-quantization integer p leads to a solution with a steeper phase profile, suggesting a more unstable situation. However, this phase effect is balanced by an increased offset a_2 of the amplitude. Qualitatively, the dynamics are as depicted in Figs. 15–16. Thus the nontrivial phase solutions of Type B are stable for $a_2 > 1/4$ and for $0 < a_2 < \sqrt{1 - k^2}/4$, whereas the nontrivial phase solution is unstable for $a_2 < -1/4$.

IV. SUMMARY AND CONCLUSIONS

We considered the repulsive nonlinear Schrödinger equation with an elliptic function potential as a model for a trapped, quasi-one-dimensional Bose-Einstein condensate. Two new families of periodic solutions of this equation were found and their stability was investigated both analytically and numerically. Using analytical results for trivial phase solutions, we showed that solutions with sufficient offset are linearly stable. Moreover, all such stable solutions are deformations of the ground state of the linear Schrödinger equation. This is confirmed with extensive numerical simulations on the governing nonlinear equation. Likewise, nontrivial phase solutions are stable if their density is sufficiently offset. Since we are

modeling a Bose-Einstein condensate trapped in a standing light wave, our results imply that a large number of condensed atoms is sufficient to form a stable, periodic condensate. Physically, this implies stability of states near the Thomas-Fermi limit.

To quantify this phenomena, we consider the $k = 0$ limit and note that from Eqs. (1) and (13), the number of particles per well n is given by $n = (\int_0^\pi |\psi(x,t)|^2 dx)/\pi = V_0/2 + B$. In the context of the BEC, and for a fixed atomic coupling strength, this means a large number of condensed atoms per well n is sufficient to provide an offset on the order of the potential strength. This ensures stabilization of the condensate. Alternatively, a condensate with a large enough number of atoms can be interpreted as a developed condensate for which the nonlinearity acts as a stabilizing mechanism.

Acknowledgments: We benefited greatly from discussions with Ricardo Carretero-González and William Reinhardt. The work of J. Bronski, L. D. Carr, B. Deconinck, and J. N. Kutz was supported by National Science Foundation Grants DMS-9972869, CHE97-32919, DMS-0071568, and DMS-9802920 respectively. K. Promislow acknowledges support from NSERC-611255

* to whom correspondence should be addressed

- [1] W. Ketterle, D. S. Sturfee, and D. M. Stamper-Kurn, in *Proceedings of the International School of Physics "Enrico Fermi"* (IOS Press, Amsterdam; Washington, D.C., 1999), pp. 67–176.
- [2] F. Dalfovo, S. Giorgini, L. P. Pitaevskii, and S. Stringari, *Rev. Mod. Phys.* **71**, 463 (1999).
- [3] K. Huang, *Statistical Mechanics*, (John Wiley, New York, 1963).
- [4] B. P. Anderson and M. A. Kasevich, *Science* **282**, 1686 (1998).
- [5] E. W. Hagley *et al.*, *Science* **283**, 1706 (1999).
- [6] M.L. Chiofalo and M.P. Tosi, *Phys. Lett. A* **268** 406 (2000).
- [7] Y. B. Ovchinnikov *et al.*, *Phys. Rev. Letts.* **83**, 284 (1999).
- [8] D. Jaksch *et al.*, *Phys. Rev. Letts.* **81**, 3108 (1998);
- [9] G. K. Brennen, C. M. Caves, P. S. Jessen, and I. H. Deutsch, *Phys. Rev. Letts.* **82**, 1060 (1999).
- [10] D.-I. Choi and Q. Niu, *Phys. Rev. Letts.* **82**, 2022 (1999).
- [11] G. Baym, *Lectures in Quantum Mechanics*, (Addison-Wesley, Redwood City, CA), Ch. 20.
- [12] L. P. Pitaevskii, *Sov. Phys. JETP* **13**, 451 (1961).
- [13] E. P. Gross, *Nuovo Cimento* **20**, 454 (1961).
- [14] D. S. Petrov, M. Holzmann, and G. V. Shlyapnikov, *Phys. Rev. Letts.* **84**, 2551 (2000).
- [15] D.S. Petrov, G.V. Shlyapnikov, and J.T.M. Walraven, e-print cond-mat/0006339 (2000).
- [16] L.D. Carr, C.W. Clark, and W.P. Reinhardt, *Phys. Rev.*

- A **62** 0436XX-1, e-print cond-mat/9911177 (2000).
- [17] L.D. Carr, M. A. Leung, and W.P. Reinhardt, J. Phys. B **33** p.xxx, e-print cond-mat/0004287 (2000).
- [18] M. Key *et al.*, Phys. Rev. Letts. **84**, 1371 (2000).
- [19] N. H. Dekker *et al.*, Phys. Rev. Letts. **84**, 1124 (2000).
- [20] J. C. Bronski, L. Carr, B. Deconinck, and J. N. Kutz, PRL
- [21] M. Kunze and *et. al*, Physica D **128**, 273 (1999).
- [22] Y. S. Kivshar, T. J. Alexander, and S. K. Turitsyn, e-print cond-mat/9907475 (1999).
- [23] K. Bongs *et al.*, cond-mat/0007381 (unpublished).
- [24] M. R. Andrews *et al.*, Science **273**, 84 (1996).
- [25] J. D. Close and W. Zhang, J. Opt. B **1**, 420 (1999).
- [26] M. R. Matthews *et al.*, Phys. Rev. Letts. **83**, 2498 (1999).
- [27] *Handbook of Mathematical Functions*, edited by M. Abramowitz and I. A. Stegun (National Bureau of Standards, Washington, D. C., 1964).
- [28] S. Theodorakis and E. Leontidis, J. Phys. A **30**, 4835 (1997).
- [29] F. Barra, P. Gaspard, and S. Rica, Phys. Rev. E **61**, 5852 (2000).
- [30] K. Berg-Sørensen and K. Mølmer, Phys. Rev. A **58**, 1480 (1998).
- [31] M. J. Steel and W. Zhang, e-print cond-mat/9810284 (1998).
- [32] *Algebro-geometric approach to nonlinear integrable equations*, E. D. Belokolos, A. I. Bobenko, V. Z. Enol'skii, A. R. Its and V. B. Matveev (Springer-Verlag, Berlin, 1994).
- [33] R. Courant and D. Hilbert, *Methods of Mathematical Physics*, (Wiley, New York, 1989).
- [34] M. I. Weinstein and J. B. Keller, SIAM J. Appl. Math. **45**, 200 (1985)